Article

Synthesis and Gas Transport Properties of Hyperbranched Polyimide–Silica Hybrid/Composite Membranes

Masako Miki [1], Hideki Horiuchi [2] and Yasuharu Yamada [3],*

[1] R&D Center for Nanomaterials and Devices, Kyoto Institute of Technology, Matsugasaki, Sakyo-Ku, Kyoto 606-8585, Japan; E-Mail: m-miki@kit.ac.jp
[2] Department of Biomolecular Engineering, Kyoto Institute of Technology, Matsugasaki, Sakyo-Ku, Kyoto 606-8585, Japan; E-Mail: hhoriuchi@starlite.co.jp
[3] Institute of Technological Research, Kanagawa University, 3-27-1 Rokkakubashi, Kanagawa-ku, Yokohama 221-8686, Japan

* Author to whom correspondence should be addressed; E-Mail: ss503522rt@kanagawa-u.ac.jp; Tel./Fax: +81-45-481-5661.

Abstract: Hyperbranched polyimide–silica hybrids (HBPI–silica HBDs) and hyperbranched polyimide–silica composites (HBPI–silica CPTs) were prepared, and their general and gas transport properties were investigated to clarify the effect of silica sources and preparation methods. HBPI–silica HBDs and HBPI–silica CPTs were synthesized by two-step polymerization of $A_2 + B_3$ monomer system via polyamic acid as precursor, followed by hybridizing or blending silica sources. Silica components were incorporated by the sol-gel reaction with tetramethoxysilane (TMOS) or the addition of colloidal silica. In HBPI-silica HBDs, the aggregation of silica components is controlled because of the high affinity of HBPI and silica caused by the formation of covalent bonds between HBPI and silica. Consequently, HBPI-silica HBDs had good film formability, transparency, and mechanical properties compared with HBPI-silica CPTs. HBPI-silica HBD and CPT membranes prepared via the sol-gel reaction with TMOS showed specific gas permeabilities and permselectivities for CO_2/CH_4 separation, that is, both CO_2 permeability and CO_2/CH_4 selectivity increased with increasing silica content. This result suggests that gas transport can occur through a molecular sieving effect of the porous silica network derived from the sol-gel reaction and/or through the narrow interfacial region between the silica networks and the organic matrix.

Keywords: hyperbranched polyimide; silica hybrid; silica composite; gas permeability; gas separation

---

1. Introduction

In order to build a sustainable society, it is necessary to develop alternative energy sources to fossil fuel, as well as renewable energy, and low environmental impact processes. In the current chemical process, the innovation of energy-saving separation technology is awaited because the mass energy consumption in the process has become a major problem. Membrane separation is one of the potential technologies to solve this problem.

Gas separation membranes can be classified into inorganic membranes and polymeric membranes. Most gas separation membranes which have been put to practical use are polymeric membranes because of their low cost and good processability. However, very often they have relatively low separation performance compared to certain inorganic membranes. On the other hand, inorganic membranes are porous membranes having nano-order fine pores and exert superior gas separation performance by means of a molecular sieving function [1].

Organic–inorganic hybrid and composite materials have received much attention and have been extensively studied for a long time as a new class of high performance materials which offers the advantages of both an organic polymer (e.g., flexibility, dielectric, ductility, and processability) and an inorganic material (e.g., rigidity, thermal stability) [2,3]. We define the terms of "hybrid" and "composite" as following: "hybrid" materials are those that have strong chemical interaction between organic and inorganic components such as covalent bonds, and "composite" materials are those that show weak or no interactions between the two components. Synthesizing polyimide–silica hybrid and composite materials and investigating their physical and gas transport properties have also received much attention [4–7]. Polyimide–silica hybrids and composites can be prepared by sol-gel processes or the addition of colloidal silica. The sol-gel reaction is achieved by addition of silicon alkoxide to polyamic acid (polyimide precursor) solution, and subsequently hydrolysis and polycondensation with an appropriate acid or base catalyst; the addition of colloidal silica is commonly just blending colloidal silica particles with the polyamic acid solution. Generally, it is said that colloidal silica has a dense structure and silica prepared via the sol-gel reaction has an amorphous three-dimensional network structure with nanopores.

The dispersion of silica components in the polyimide matrix has a significant impact on the properties of hybrids and composites. The modification of polyimide molecular terminals is one of the most effective methods to enhance the compatibility between polyimide and silica and, thereby, to improve the dispersibility of the silica components. Hybrids and composites can be obtained by use of polyimide with and without terminal modification, respectively. Another effective method to improve the dispersibility is to use dendrimers or hyperbranched polymers with a highly branched structure. Hyperbranched polymers, which are a kind of dendritic polymer, attract much attention as high-performance polymers possessing unique properties compared to their linear analogues. They have good solubility, reduced viscosity, higher fractional free volume (FFV), and multifunctionality,

which arise from the multiple end groups. The most remarkable characteristic of hyperbranched polymers is that they have a large number of molecular terminal groups that can be modified to create different types of multifunctional polymers [8,9]. In addition, hyperbranched polymers have a high FFV which affects the high gas permeability and a highly branched structure which facilitates the fine dispersion of silica particles.

In our previous research, we studied the syntheses and gas transport properties of hyperbranched polyimide–silica hybrid membranes prepared with commercially available dianhydride monomers and several kinds of triamine monomers, and found that these membranes showed characteristics quite different from the conventional linear type polyimide membranes. Specifically, the gas permeability and the CO_2/CH_4 selectivity of hyperbranched polyimide–silica hybrid membranes prepared via the sol-gel reaction using tetramethoxysilane (TMOS) increased with increasing silica content without any dependence on the molecular structure, suggesting the characteristic distribution and interconnectivity of free volume holes created by the incorporation of silica [10–15].

In this study, the physical and gas transport properties of hyperbranched polyimide–silica hybrid (HBPI–silica HBD) and hyperbranched polyimide–silica composite (HBPI–silica CPT) membranes prepared with silicon alkoxide (TMOS) or colloidal silica were investigated to clarify the differences as well as the gas transport mechanism in the HBPI–silica HBD and CPT membranes.

2. Experimental Section

2.1. Materials

1,3,5-Tris(4-aminophenoxy)benzene (TAPOB) was synthesized by the reduction of 1,3,5-tris(4-nitrophenoxy)benzene with palladium carbon and hydrazine in methanol [16]. Dianhydride, 4,4′-(hexafluoroisopropylidene) diphthalic anhydride (6FDA) was kindly supplied by Daikin Industries (Osaka, Japan). 3-Aminopropyltrimethoxysilane (APTrMOS) was purchased from Sigma-Aldrich Co. LLC. (St. Louis, MO, USA). TMOS was purchased from AZmax, Co., Ltd. (Tokyo, Japan) and colloidal silica was obtained from Nissan chemical industries, LTD. (Tokyo, Japan). *N,N*-Dimethylacetamide (DMAc) used as a solvent was purchased from Nacalai Tesque (Kyoto, Japan). The chemical structures of the monomers, silane coupling agents, and silica sources are shown in Figure 1.

Figure 1. Chemical structures of the monomers, silane coupling agents, and silica sources.

1,3,5-Tris(4-aminophenoxy)benzene

(TAPOB)

4,4'-(Hexafluoroisopropylidene) diphthalic anhydride

(6FDA)

3-Aminopropyltrimethoxysilane

(APTrMOS)

Tetramethoxysilane

(TMOS)

Colloical silica

(particle diameter: 10-20 nm)
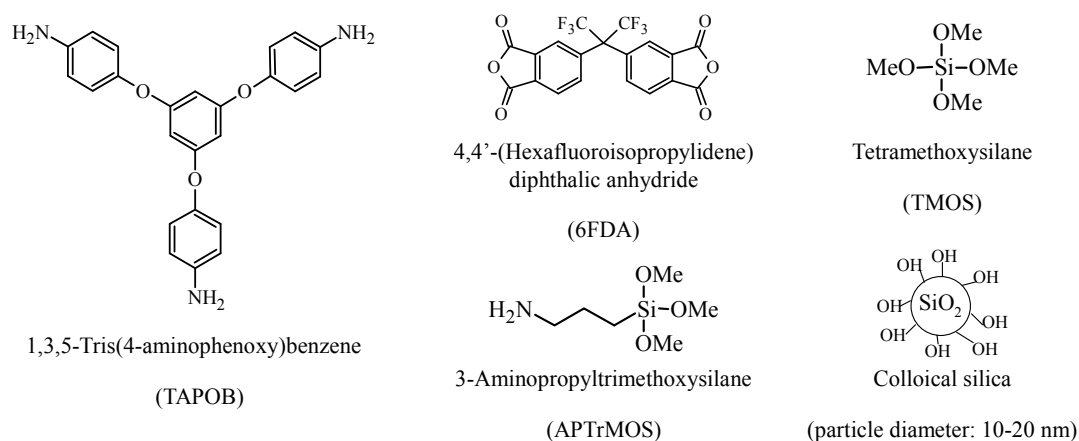
2.2. Polymerization

Three mmol of 6FDA was dissolved in 40 mL of DMAc in a 100 mL three-neck flask under N_2 flow at room temperature. To this solution, 1.6 mmol of TAPOB in 20 mL of DMAc was then added dropwise through a syringe with stirring for 3 h to afford hyperbranched polyamic acids (HBPAAs). Subsequently, for the HBPAAs to be used for the preparation of HBPI–silica HBDs, 0.4 mmol of the silane coupling agent, APTrMOS, was added into the reaction mixture to modify the end groups of the HBPAAs with further stirring for 1 h.

2.3. Membrane Formation

2.3.1. HBPI–Silica HBD and HBPI–Silica CPT Prepared via Sol-Gel Reaction with TMOS

The HBPI–silica HBDs and HBPI–silica CPTs prepared via sol-gel reaction with TMOS were prepared to react HBPAAs with silicon alkoxide, TMOS, by sol-gel reaction, and then followed by thermal imidization. Appropriate amounts of TMOS and deionized water (TMOS: deionized water = 1:6 as a molar ratio) were added into the DMAc solution of the HBPAAs. HBPAAs modified with APTrMOS were used for the preparation of HBPI–silica HBDs prepared via sol-gel reaction with TMOS, and on the other hand, unmodified HBPAAs were used for the preparation of HBPI–silica CPTs prepared via sol-gel reaction with TMOS. The mixed solutions were stirred for 24 h and then cast on polyethylene terephthalate films and dried at 85 °C for 3 h. The prepared membranes were peeled off and subsequently imidized at 100 °C for 1 h, 200 °C for 1 h, and 300 °C for 1 h in a heating oven under N_2 flow. The composition of the prepared membranes was listed in Table 1.

Table 1. The composition of the prepared membranes.

Type of hybrid/composite	HBPI	Preparation method	Silica source	
			Starting material	**Content (wt %)**
TMOS system HBPI–silica HBD	modified HBPI	hybrid	TMOS	0, 10, 20, 30
TMOS system HBPI–silica CPT	unmodified HBPI	composite	TMOS	0, 10, 20, 30
colloidal silica system HBPI–silica HBD	modified HBPI	hybrid	colloidal silica	0, 10, 20, 30
colloidal silica system HBPI–silica CPT	unmodified HBPI	composite	colloidal silica	0, 10, 20, 30

Notes: TMOS: tetramethoxysilane; HBPI: hyperbranched polyimide; HBD: hybrid; CPT: composite.

2.3.2. HBPI–Silica HBD with Colloidal Silica and HBPI-Silica CPT with Colloidal Silica

The HBPI–silica HBDs with colloidal silica and HBPI–silica CPTs with colloidal silica were prepared by blending HBPAAs and colloidal silica, followed by thermal imidization. Appropriate amounts of colloidal silica dispersed in DMAc were added into the DMAc solution of the HBPAAs. As is the case with the TMOS system, on the one hand HBPAAs modified with APTrMOS were used for the preparation of HBPI–silica HBD with colloidal silica, and on the other hand, unmodified HBPAAs were used for the preparation of HBPI–silica CPT with colloidal silica. Shortly after mixing the HBPAAs and colloidal silica, the prepared solutions were cast on PET films and dried at 85 °C for

3 h. The prepared membranes were peeled off and subsequently imidized at 100 °C for 1 h, 200 °C for 1 h, and 300 °C for 1 h in a heating oven under N_2 flow. The composition of the prepared membranes is listed in Table 1.

2.4. Measurements

Attenuated total reflection Fourier transform infrared (ATR FT-IR) spectra were recorded on a JASCO (Tokyo, Japan) FT/IR-4100 at a wavenumber range of 550–4000 cm^{-1} and a resolution of 1 cm^{-1}. Ultraviolet-visible (UV-vis) optical transmittances were measured with a JASCO (Tokyo, Japan) V-530 UV/vis spectrometer at wavelengths of 200–800 nm. Thermogravimetric-differential thermal analysis (TG-DTA) experiments were performed with a Seiko Instruments (Chiba, Japan) TG/DTA5200 at a heating rate of 10 °C/min under air flow. Dynamic mechanical analysis (DMA) measurements were performed with a Seiko Instruments (Chiba, Japan) DMA6100 at a heating rate of 5 °C/min under N_2 flow; the load frequency was 1 Hz. Thermal mechanical analysis (TMA) measurements were carried out using a Seiko Instruments (Chiba, Japan) TMA/SS6100 at a heating rate of 5 °C/min under N_2 flow. CO_2, O_2, N_2 and CH_4 permeation measurements were taken with a constant volume/variable pressure apparatus under 76 cmHg at 25 °C. The permeability coefficient, P [$cm^3 \cdot (STP) \cdot cm/cm^2 \cdot s \cdot cmHg$], was determined by the equation [17]:

$$P = \frac{22414}{A} \frac{L}{p} \frac{V}{RT} \frac{dp}{dt} \tag{1}$$

where A is the membrane area (cm^2), L is the membrane thickness (cm), p is the upstream pressure (cmHg), V is the downstream volume (cm^3), R is the universal gas constant (6236.56 $cm^3 \cdot cmHg/mol \cdot K$), T is the absolute temperature (K), and dp/dt is the permeation rate (cmHg/s). The gas permeability coefficient can be explained on the basis of the solution-diffusion mechanism, which is represented by the equation [18,19]:

$$P = D \times S \tag{2}$$

where D (cm^2/s) is the diffusion coefficient and S [cm^3 (STP)/cm^3 polym cmHg] is the solubility coefficient. The diffusion coefficient was calculated by the time-lag method represented by the equation [20]:

$$D = \frac{L^2}{6\theta_t} \tag{3}$$

where θ_t (s) is the time-lag.

Wide angle X-ray diffractometry (WAXD) measurements were recorded at room temperature by using Rigaku (Tokyo, Japan) RINT2500 in the 2θ range of 5°–40° with a scan rate of 2°/min. Cu K_α (wavelength $\lambda = 0.154$ nm) radiation was used. The average d-spacing value was determined from Bragg's equation:

$$d = \frac{\lambda}{2\sin\theta}$$

$$\alpha(A/B) = \frac{P(A)}{P(B)} = \frac{D(A)}{D(B)} \times \frac{S(A)}{S(B)} = \alpha^D(A/B) \times \alpha^S(A/B) \tag{4}$$

3. Results and Discussion

3.1. Polymer Characterization

The ATR FT-IR spectra of the HBPI–silica HBD and CPT films are shown in Figure 2a,b. The bands observed around 1784 cm^{-1} (C=O asymmetrical stretching), 1722 cm^{-1} (C=O symmetrical stretching), 1375 cm^{-1} (C–N stretching), and 720 cm^{-1} (C=O bending) are characteristic absorption bands of polyimides. In contrast, the characteristic band of polyamic acids around 1680 cm^{-1} is not found. These results indicate that the prepared membranes are well imidized. The bands around 1857 cm^{-1} are attributed to the stretching of C=O of the terminal anhydride groups in the HBPI molecules [21,22]. For the HBPI–silica HBDs prepared via sol-gel reaction with TMOS, it can be observed that the broad and strong absorption bands around 1100 cm^{-1} assigned to Si–O–Si stretching are enhanced with increasing SiO$_2$ content (Figure 2a), indicating sufficient formation of the three-dimensional Si–O–Si network [23]. The broad absorption bands around 3480 cm^{-1} are likely attributable to silanol groups remaining in the silica domain. In comparison toof the TMOS system and colloidal silica system (Figure 2b), the absorption bands around 3480 cm^{-1} of the TMOS system are stronger than that of colloidal silica system, suggesting that many more silanol groups remain in the TMOS system than in the colloidal silica system. It is also recognizable that the absorption bands around 1100 cm^{-1} of the colloidal silica system are sharper and shifted slightly toward high wavenumber region than that of the TMOS system, suggesting rigid Si-O-Si bondings in the colloidal silica system.

Figure 2. Attenuated total reflection Fourier transform infrared (ATR FT-IR) spectra of the (**a**) Hyperbranched polyimide–silica hybrids (HBPI–silica HBDs) prepared via sol-gel reaction with TMOS (SiO$_2$ content: 0–30 wt %); and (**b**) HBPI–silica HBDs and hyperbranched polyimide–silica composites (HBPI–silica CPTs) (SiO$_2$ content: 30 wt %).
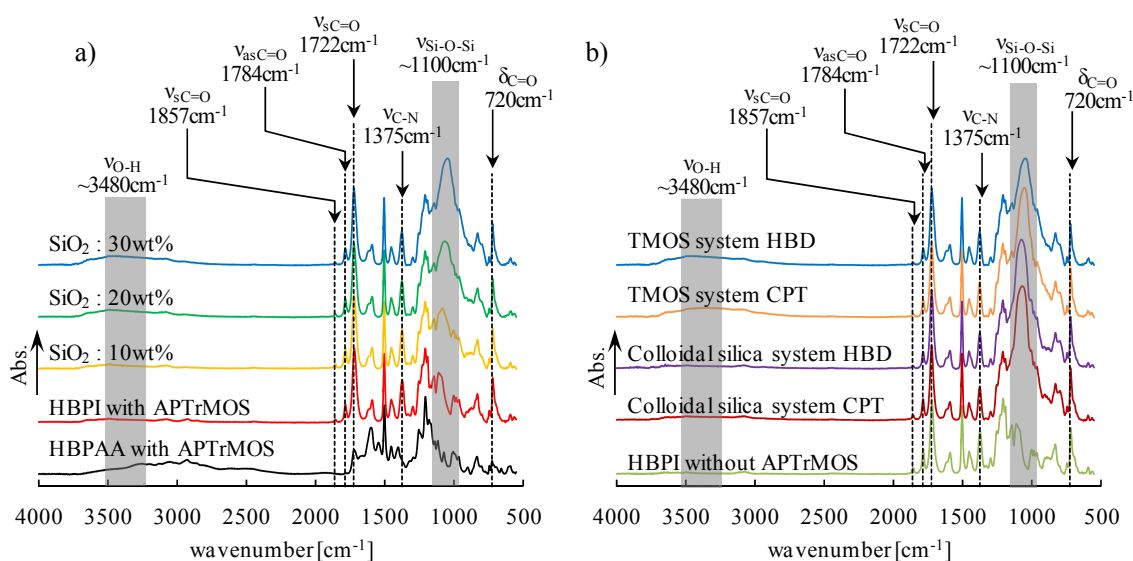
The optical transmittances at 600 nm are shown in Table 2. The hybrid films maintain high transparency similar to the corresponding pristine HBPIs up to a high silica content. This result might be attributed to the decreased imide group density in a unit volume and favorably fine dispersion of

silica without aggregation. The fine and homogeneous dispersion of silica in the hybrid films is brought about by the silane coupling agents which offer covalent bonds between the organic and inorganic components [24]. On the other hand, the transparency of the composite films decreased severely with increasing silica content. This probably results from the low affinity of HBPI and the silica moiety which leads to the aggregation of the silica components, consequently light scattering occurs in the visible light region.

**Table 2.** Physical properties of HBPI–silica hybrid and composite films.

Type of HBPI and hybrid/composite	Silica content	Transmittance at 600 nm (%)	TG-DTA		DMA	TMA
			T_d^5 (°C)	Residue (%)	T_g (°C)	CTE (ppm/°C)
Modified HBPI	–	88.9	457	0	304	56
TMOS system HBD	10 wt % SiO$_2$	89.9	490	10	320	47
	20 wt % SiO$_2$	90.2	496	20	338	31
	30 wt % SiO$_2$	90.3	509	30	351	25
Colloidal silica system HBD	10 wt % SiO$_2$	88.5	477	9	299	47
	20 wt % SiO$_2$	89.4	482	19	299	40
	30 wt % SiO$_2$	89.5	488	30	304	36
Unmodified HBPI	–	90.8	499	0	281	51
TMOS system CPT	10 wt % SiO$_2$	84.1	478	10	284	42
	20 wt % SiO$_2$	78.2	488	18	285	33
	30 wt % SiO$_2$	79.4	500	29	289	25
Colloidal silica system CPT	10 wt % SiO$_2$	76.9	479	9	279	44
	20 wt % SiO$_2$	71.4	484	17	282	38
	30 wt % SiO$_2$	69.8	491	28	287	31

Notes: TG-DTA: thermogravimetric-differential thermal analysis; T_d^5: 5% weight-loss temperature; DMA: dynamic mechanical analysis; T_g: glass transition temperature; TMA: Thermal mechanical analysis; CTE: coefficients of thermal expansion.

The thermal properties of the HBPI–silica HBDs and CPTs were investigated by TG-DTA, DMA and TMA measurements. The 5% weight-loss temperatures (T_d^5s) of the HBPI–silica hybrid membranes were investigated by TG-DTA and are summarized in Table 2 along with the silica content determined from the residues at 800 °C. The residues showed that all hybrid membranes contained an appropriate amount of silica, as expected. In Figure 3, the T_d^5 values of the HBPI–silica HBDs and CPTs are plotted against silica content. The T_d^5 of the pristine HBPI modified with APTrMOS was lower than that of the unmodified pristine HBPI, because C–N bonds formed by the addition of APTrMOS are less thermally stable [15]. The T_d^5 values of the HBPI–silica HBDs increased with increasing silica content due to the formation of crosslinks between HBPI and the silica domain, the introduction of inorganic characteristics, and the radical trap effect of silica. Of particular note, the T_d^5 values of the HBPI–silica HBDs prepared via sol-gel reaction with TMOS which contain many silanol groups remarkably increased because of the significant contribution of the formation of crosslinks between HBPI and the silica domain. For the colloidal silica system, the crosslinking reaction occurs with

difficulty because there are not so many silanol groups on the surface of silica particles as silica prepared via the sol-gel reaction. In the HBPI–silica CPTs, the T_d^5 values of both TMOS and the colloidal silica system decreased in the low silica content region. This result might arise from the influence of dehydration from unreacted silanol groups in the silica domain derived from the sol-gel reaction or on the surface of the silica particle. By contrast, in the higher silica content region, the T_d^5 values of both TMOS and the colloidal silica system increased with increasing silica content due to the strong influence of the introduction of inorganic characteristics, and the radical trap effect of silica.

Figure 3. Five percent weight loss temperatures (T_d^5s) of HBPI–silica HBDs and CPTs.
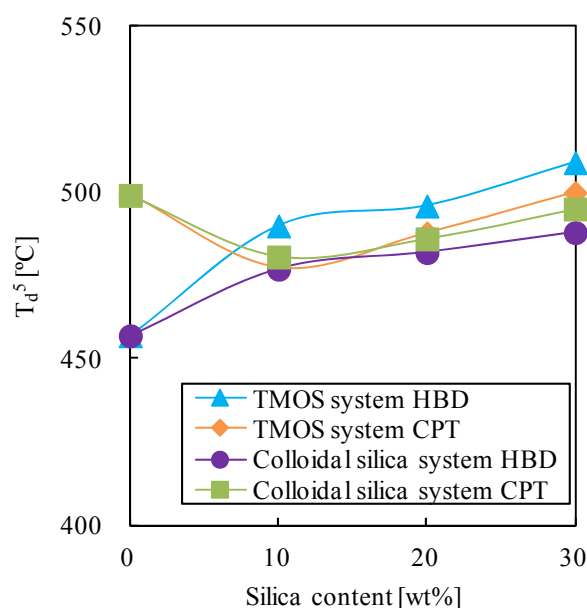
The storage moduli (E's) and tan δ of the HBPI–silica HBD and CPT films are shown in Figure 4a–d and E's in the rubbery region and glassy region are plotted against the silica content in Figure 5a,b. In the glassy region, no remarkable difference between these films was observed. In contrast, in the rubbery region, the E's of the TMOS system HBPI–silica HBD films were clearly higher than those of the other corresponding films. This result indicates that in the rubbery region, the mobility of the molecular chains of the TMOS system HBPI–silica HBD is much lower than others because many more covalent bonds are formed between modified HBPI and the silica moiety prepared via the sol-gel reaction. This result also supports the above mentioned discussion about the T_d^5 behavior. The glass transition temperatures (T_gs) of the HBPI–silica HBD and CPT films determined from the peak of tan δ are summarized in Table 1 and plotted against the silica content in Figure 6. Although the decrease of the peak intensity and the broadening of the half-width of tan δ were recognized for all of the examined films, the shift of T_g (peak top of the tan δ) to a higher temperature was observed only for the HBPI–silica HBDs prepared via the sol-gel reaction with TMOS. This result is also due to the difference in the affinity of the HBPI molecular chain and the silica moiety; the molecular mobility decreased in HBPI–silica HBDs prepared via the sol-gel reaction with TMOS, resulting from the strong interaction between the two components through much crosslinking.

Figure 4. Storage modulus (E') and tan δ of (**a**) HBPI–silica HBD films prepared via the sol-gel reaction with TMOS; (**b**) HBPI–silica CPT films prepared via the sol-gel reaction with TMOS; (**c**) HBPI–silica HBD films with colloidal silica; and (**d**) HBPI–silica CPT films with colloidal silica.
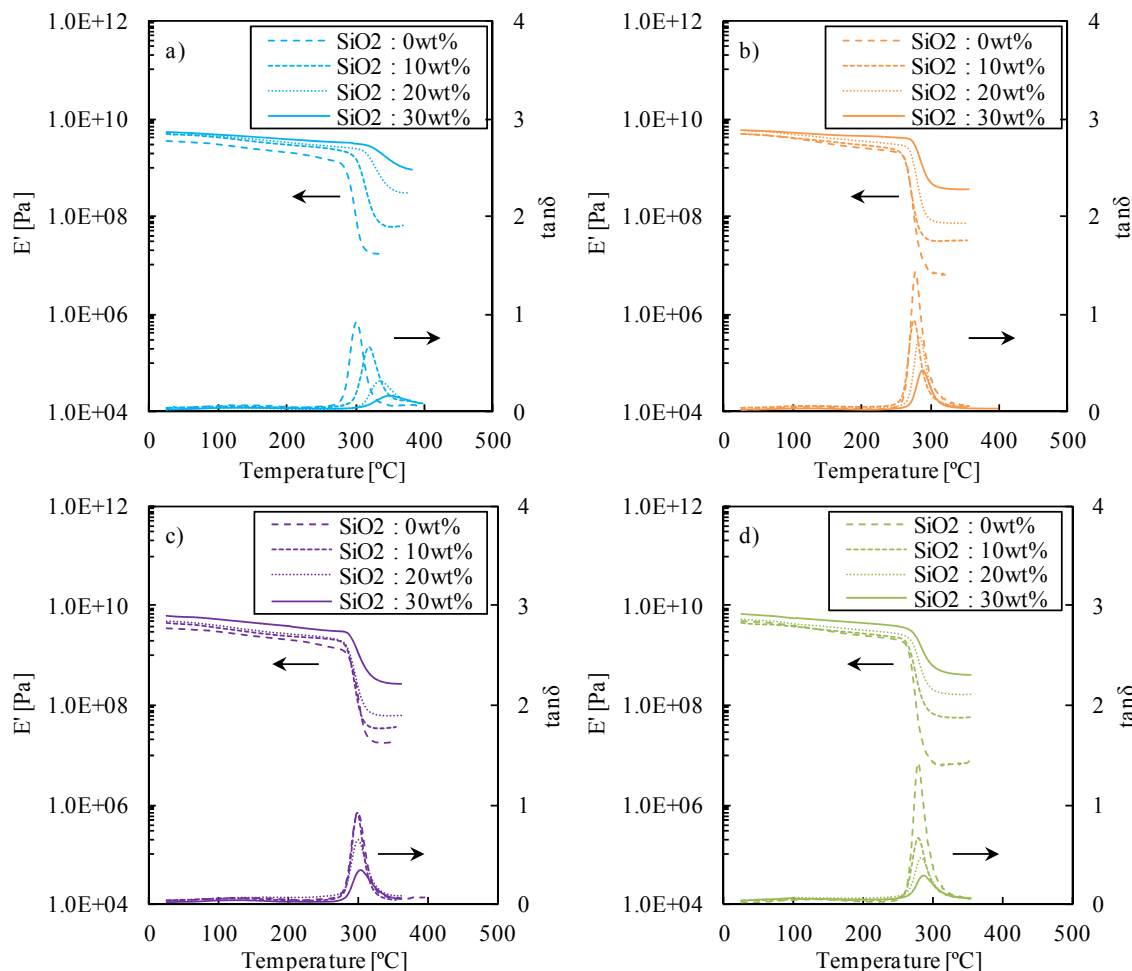

Figure 5. E' in the (**a**) rubbery region and (**b**) glassy region of HBPI–silica HBD and CPT films plotted against silica content.
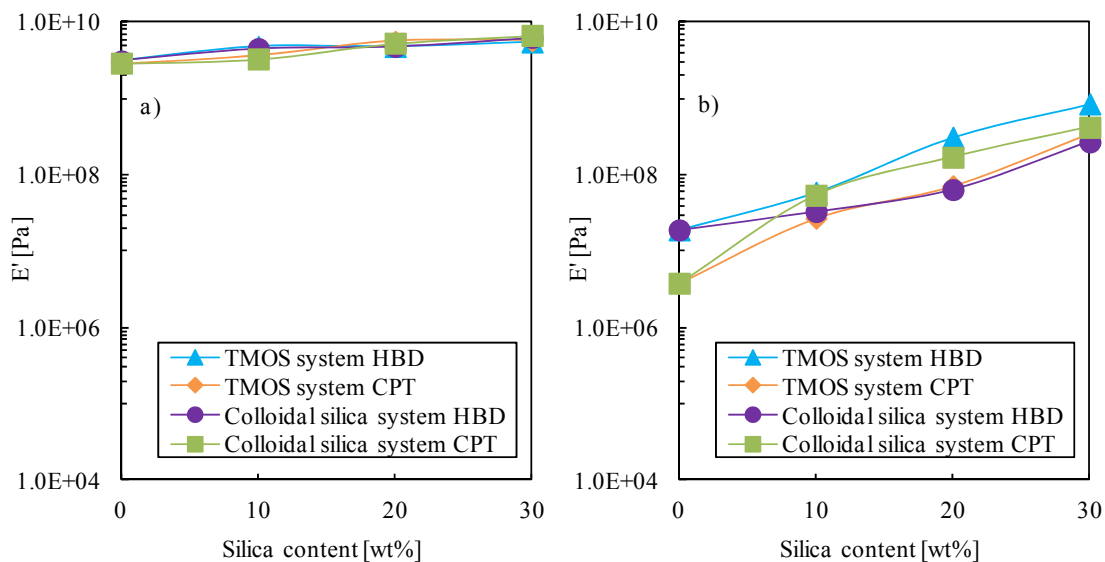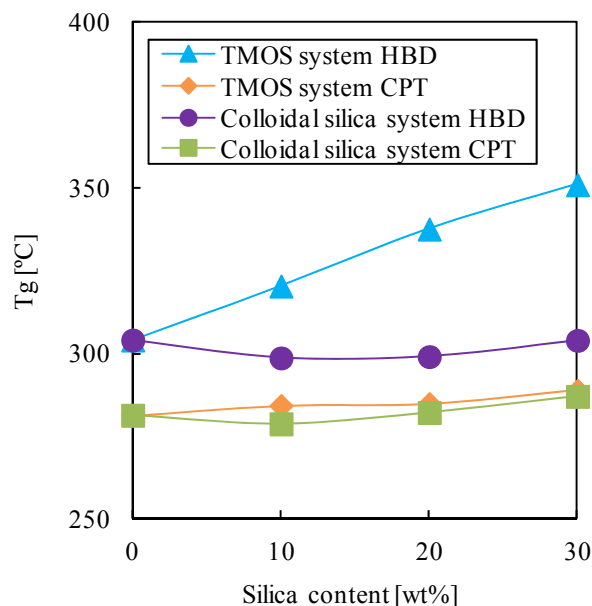
Figure 6. Glass transition temperatures (T_gs) of HBPI–silica HBD and CPT films derived from the peak of tan δ.

The coefficients of thermal expansion (CTEs) from 100 to 150 °C of the HBPI–silica HBD and CPT films are listed in Table 2. The CTEs of all hybrid and composite films decreased with increasing silica content attributed to the introduction of inorganic characteristics. In the TMOS system, the CTEs decreased conspicuously without dependence on hybrids or composites because the inorganic characteristics of the silica domain appear strong due to the three-dimensional entanglement of the HBPI molecules and the silica moiety.

3.2. Gas Transport Properties

3.2.1. Gas Permeability

The gas permeability, diffusion, and solubility coefficients of the HBPI–silica HBD and CPT membranes are summarized in Table 3, and the CO_2 permeability, diffusion, and solubility coefficients are plotted against the silica content in Figure 7a–c. As shown in Table 3 and Figure 7, the gas permeability coefficients of the HBPI–silica HBD and CPT membranes prepared via the sol-gel reaction with TMOS increased with increasing silica content due to the contributions of the diffusion coefficient and the solubility coefficient. This result indicates the additional formation of free-volume holes and a Langmuir sorption site effective for gas transport properties through hybridization or composition with silica [14,25,26]. By contrast, the gas permeability coefficients of the HBPI–silica HBD and CPT membranes prepared with colloidal silica increased very little with increasing silica content. From these results, it was revealed that the gas transport behavior of the HBPI–silica HBD and CPT membranes was controlled largely by a silica source (sol-gel reaction with TMOS or colloidal silica) than the preparation method (hybrid or composite). Generally, it is well known that the introduction of dense inorganic particles to a polymer matrix increases the gas barrier properties of the polymer films. For example, the permeability coefficient of the composite membrane with only 2 wt % addition of montmorillonite is less than half of that of pristine polyimide for various gases. This decrease in

permeability coefficients was explained by the increase of the total path of gas [27]. Gases cannot diffuse through the dense inorganic filler. On the other hand, Park *et al.* pointed out that the gas transport of siloxane containing polyimide membrane could occur through the porous silica network and/or the path in the interfacial region between the silica networks and the organic matrix [28]. Similar gas transport properties have been reported in several other studies. Merkel *et al.* reported increased gas permeabilities of a high-free-volume glassy polymer due to the incorporation of nanosilica particles. They concluded that the polymer chains around the nanosilica particles were unable to pack efficiently, resulting in a low-density polymer-nanoparticle interfacial region which allows permeation of gases [29–31]. Hill suggested a theoretical model to quantitatively interpret the experiments of Merkel *et al.* [32,33]. He concluded that the incorporation of nanoinclusion leads to the formation of a polymer-segment depletion layer at the inclusion-polymer interface, and that the accompanying increase in free volume increased the bulk permeability and selectivity due to a significant increase in the local penetrant diffusivity. Zhang *et al.* also reported the improvement of the permeability of poly(vinyl alcohol)/1,2-bis(triethoxysilyl)ethane hybrid membranes, and suggested that the amorphous region in the hybrid membranes increased with increasing silica content [34]. The increased solubilities of the HBPI–silica HBD and CPT membranes prepared via the sol-gel reaction with TMOS suggest that the Langmuir-type sorption site is additionally formed by the incorporation of silica domains. There are so many sorption sites in the HBPI–silica HBD and CPT membranes prepared via the sol-gel reaction with TMOS because the silica domain prepared via the sol-gel reaction is porous and its specific surface area is large [35].

Table 3. Gas transport properties of HBPI–silica hybrid membranes at 76 cmHg and 25 °C.

Type of HBPI and hybrid/composite	Silica content	$P \times 10^{10}$ [cm³ (STP) cm/cm² s cmHg]				$D \times 10^8$ [cm²/s]				$S \times 10^2$ [cm³ (STP)/cm³ polym cmHg]			
		CO₂	O₂	N₂	CH₄	CO₂	O₂	N₂	CH₄	CO₂	O₂	N₂	CH₄
Modified HBPI	–	7.4	1.5	0.23	0.098	0.30	1.4	0.25	0.028	25	1.1	0.92	3.5
TMOS system HBD	10 wt % SiO₂	10	2.0	0.31	0.13	0.35	1.5	0.29	0.026	30	1.4	1.1	5.0
	20 wt % SiO₂	13	2.1	0.32	0.16	0.37	1.3	0.25	0.030	35	1.7	1.3	5.2
	30 wt % SiO₂	23	3.0	0.46	0.24	0.57	1.7	0.29	0.040	41	1.8	1.6	6.0
Colloidal silica system HBD	10 wt % SiO₂	8.0	1.7	0.27	0.12	0.42	1.8	0.33	0.048	19	0.97	0.80	2.5
	20 wt % SiO₂	8.1	1.6	0.30	0.12	0.37	1.5	0.33	0.049	22	1.1	0.91	2.5
	30 wt % SiO₂	8.4	1.9	0.27	0.13	0.40	1.6	0.35	0.041	21	1.3	0.77	3.2
Unmodified HBPI	–	3.8	0.86	0.11	0.046	0.19	0.87	0.14	0.012	21	0.99	0.81	3.9
TMOS system CPT	10 wt % SiO₂	4.9	1.0	0.13	0.048	0.23	0.95	0.15	0.011	22	1.1	0.88	4.3
	20 wt % SiO₂	7.0	1.3	0.18	0.067	0.25	0.97	0.16	0.012	28	1.4	1.1	5.4
	30 wt % SiO₂	17	2.7	0.39	0.13	0.51	1.8	0.29	0.026	33	1.5	1.4	5.0
Colloidal silica system CPT	10 wt % SiO₂	4.8	1.1	0.15	0.063	0.23	1.1	0.19	0.021	21	0.96	0.77	3.0
	20 wt % SiO₂	4.9	1.1	0.15	0.066	0.26	1.0	0.21	0.022	19	1.0	0.71	3.0
	30 wt % SiO₂	5.1	1.1	0.15	0.070	0.26	1.1	0.21	0.023	20	0.97	0.74	3.0

Figure 7. CO_2 (**a**) permeability; (**b**) diffusion; and (**c**) solubility coefficients of HBPI–silica HBD and CPT membranes.
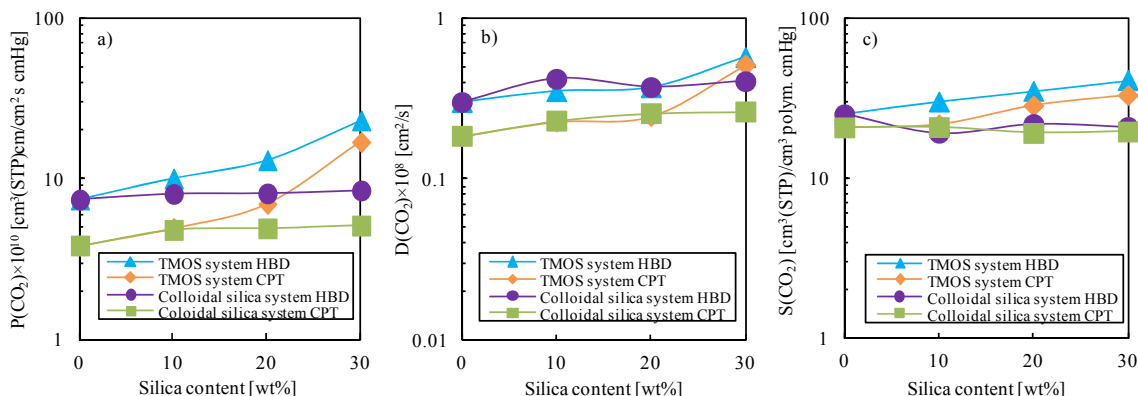

3.2.2. Gas Selectivity

The ideal selectivity for the combination of gases A and B [α(A/B)] is defined by the following Equation (5) [36]:

$$\alpha(A/B) = \frac{P(A)}{P(B)} = \frac{D(A)}{D(B)} \times \frac{S(A)}{S(B)} = \alpha^D(A/B) \times \alpha^S(A/B) \tag{5}$$

where α^D(A/B) is the diffusivity selectivity and α^S(A/B) is the solubility selectivity. The O_2/N_2 and CO_2/CH_4 selectivities of the HBPI–silica hybrid membranes are listed in Table 4, and $\alpha(CO_2/CH_4)$ is plotted against the CO_2 permeability coefficients in Figure 8. In Table 4, the O_2/N_2 selectivity slightly decreased with increasing O_2 permeability. This behavior is consistent with the general understanding that more permeable polymers are generally less selective, and *vice versa* [36]. Hence, it can be concluded that free volume holes formed by hybridization or composition with silica are not sufficiently effective to separate O_2 and N_2 that have similar kinetic diameters and shapes. For the CO_2/CH_4 selectivity, in Figure 8, we can see the different tendencies depending on the silica source. $\alpha(CO_2/CH_4)$ of the HBPI–silica HBD and CPT with colloidal silica slightly decreasing with increasing CO_2 permeability along with the upper bound trade-off line for CO_2/CH_4 separation demonstrated by Robeson [37,38], suggesting that the free volume formed in the colloidal silica system is not competent to separate CO_2 and CH_4. By contrast, both the CO_2 permeability and the CO_2/CH_4 selectivity of the HBPI–silica HBD and CPT membranes prepared via the sol-gel reaction with TMOS increased with increasing silica content. This result revealed that the free volume having CO_2/CH_4 separation ability was formed by hybridization or composition with silica in the TMOS system.

Table 4. O_2/N_2 and CO_2/CH_4 selectivities of HBPI–silica hybrid membranes at 76 cmHg and 25 °C.

Type of HBPI and hybrid/composite	Silica content	O_2/N_2 Selectivity			CO_2/CH_4 Selectivity		
		$\alpha(O_2/N_2)$	$\alpha^D(O_2/N_2)$	$\alpha^S(O_2/N_2)$	$\alpha(CO_2/CH_4)$	$\alpha^D(CO_2/CH_4)$	$\alpha^S(CO_2/CH_4)$
Modified HBPI	–	6.8	5.8	1.2	75	11	7.0
TMOS system HBD	10 wt % SiO_2	6.6	5.2	1.3	79	13	5.9
	20 wt % SiO_2	6.7	5.3	1.3	82	12	6.8
	30 wt % SiO_2	6.6	5.8	1.1	95	14	6.7
Colloidal silica system HBD	10 wt % SiO_2	6.5	5.5	1.2	67	8.8	7.6
	20 wt % SiO_2	5.4	4.4	1.2	66	7.6	8.7
	30 wt % SiO_2	7.2	4.4	1.6	64	9.9	6.5
Unmodified HBPI	–	7.8	6.4	1.2	83	15	5.3
TMOS system CPT	10 wt % SiO_2	7.9	6.3	1.2	102	20	5.0
	20 wt % SiO_2	7.3	6.0	1.2	104	20	5.3
	30 wt % SiO_2	7.0	6.2	1.1	129	20	6.6
Colloidal silica system CPT	10 wt % SiO_2	7.1	5.7	1.3	76	11	6.9
	20 wt % SiO_2	7.2	5.0	1.5	74	11	6.4
	30 wt % SiO_2	7.0	5.4	1.3	73	11	6.5

**Figure 8.** Ideal CO_2/CH_4 permselectivity [$\alpha(CO_2/CH_4)$] of HPBI–silica HBD and CPT membranes plotted against CO_2 permeability coefficient.
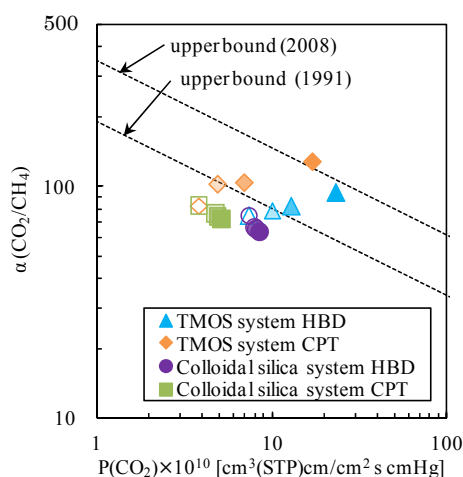
3.2.3. Wide angle X-ray Diffractometry (WAXD) Measurements

WAXD measurements were performed to scrutinize the difference between the TMOS system and the colloidal silica system. Figure 9 shows the diffraction patterns of (a) pristine HBPI; (b) HBPI–silica HBDs prepared via the sol-gel reaction with TMOS; and (c) HBPI–silica HBDs prepared with colloidal silica. In the spectrum of the HBPI base polymer, a broad peak was found around $2\theta = 15.0°$. The *d*-spacings can be calculated by applying the scattering angles (2θ) of the peaks into the Bragg's equation, $n\lambda = 2d \sin \theta$. The *d*-spacings determined from this manner represent the approximate average intersegmental distance of polymeric molecules [39–41]. Both TMOS system and colloidal silica system hybrids show two diffraction peaks. From Figure 9b,c, the intersegmental

distance (*d*-spacing) of the HBPI molecule is narrowed by hybridization with silica derived from TMOS, whereas, it is slightly spread by hybridization with colloidal silica. The narrowing of the intersegmental distance in the HBPI–silica HBD with silica derived from TMOS may arise from the crosslinks formed between the HBPI molecular terminal and silanol groups remaining in the silica domain. On the other hand, the *d*-spacing of the HBPI molecule in the colloidal silica system HBPI–silica HBDs is expanded slightly more than in pristine HBPI because the nanosilica particles disrupt the polymer chain packing. The peak around 21°–24° is caused by diffraction of the silica moiety. It was confirmed that the silica domains prepared via the sol-gel reaction with TMOS were more amorphous than the colloidal silica due to the lower and broader peak of the WAXD pattern. Comparing the *d*-spacing attributed to the silica moiety and the kinetic diameters of studied gases (CO_2: 3.3 Å, O_2: 3.5 Å, N_2: 3.6 Å, CH_4: 3.8 Å), it cannot be denied that the gases permeate through the amorphous silica prepared by the sol-gel reaction that has a molecular sieving function.

Figure 9. Wide angle X-ray diffractometry (WAXD) patterns of (**a**) pristine HBPI; (**b**) HBPI–silica HBDs prepared via sol-gel reaction with TMOS (SiO_2 content: 30 wt %); and (**c**) HBPI–silica HBDs prepared with colloidal silica (SiO_2 content: 30 wt %).
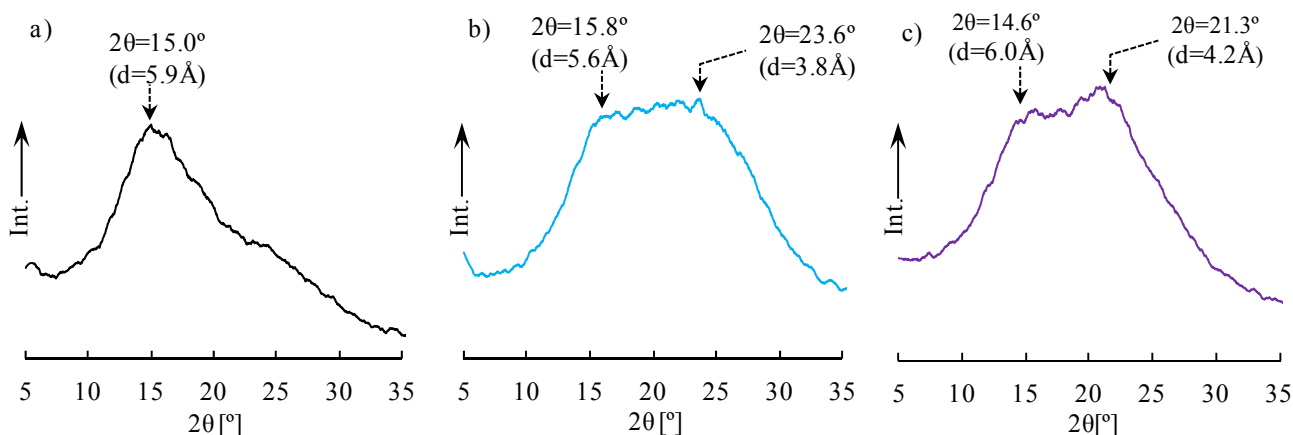

3.3. Gas Transport Mechanism

From the results of gas permeability and selectivity in the HBPI–silica HBD and CPT membranes, we considered the gas transport mechanism in the HBPI–silica HBD and CPT membranes as shown in Figure 10.

In the HBPI–silica HBD and CPT membranes prepared via the sol-gel reaction, gases can permeate through not only the newly formed diffusion path around the HBPI–silica interfacial region but also inside the porous nanosilica components because the amorphous silica is formed by the sol-gel reaction. Consequently, the gas permeability increases with increasing silica content. Furthermore, the CO_2/CH_4 selectivity of the HBPI–silica HBD and CPT membranes increased with increasing silica content because the porous nanosilica formed by the sol-gel reaction has molecular sieving effects.

On the other hand, in the HBPI–silica HBD and CPT membranes prepared with colloidal silica, large voids without CO_2/CH_4 separation ability are formed around the HBPI–silica interfacial region because of the weak interaction of HBPI and silica nanoparticles. Gases permeate a tortuous diffusion path formed between HBPI and the silica component since they cannot permeate through the dense

colloidal silica phase. Therefore, few effects were found in the permeability and CO_2/CH_4 selectivity in the HBPI–silica HBD and CPT membranes prepared with colloidal silica.

Figure 10. Schematic image of gas transport mechanism through (**a**) TMOS system hyperbranched polyimide–silica hybrid (HBPI–silica HBD); (**b**) TMOS system hyperbranched polyimide–silica composites (HBPI–silica CPT); (**c**) colloidal silica system HBPI–silica HBD, and (**d**) colloidal silica system HBPI–silica CPT membranes.

a) TMOS system HBD

b) TMOS system CPT

c) Colloidal silica system HBD

d) Colloidal silica system CPT
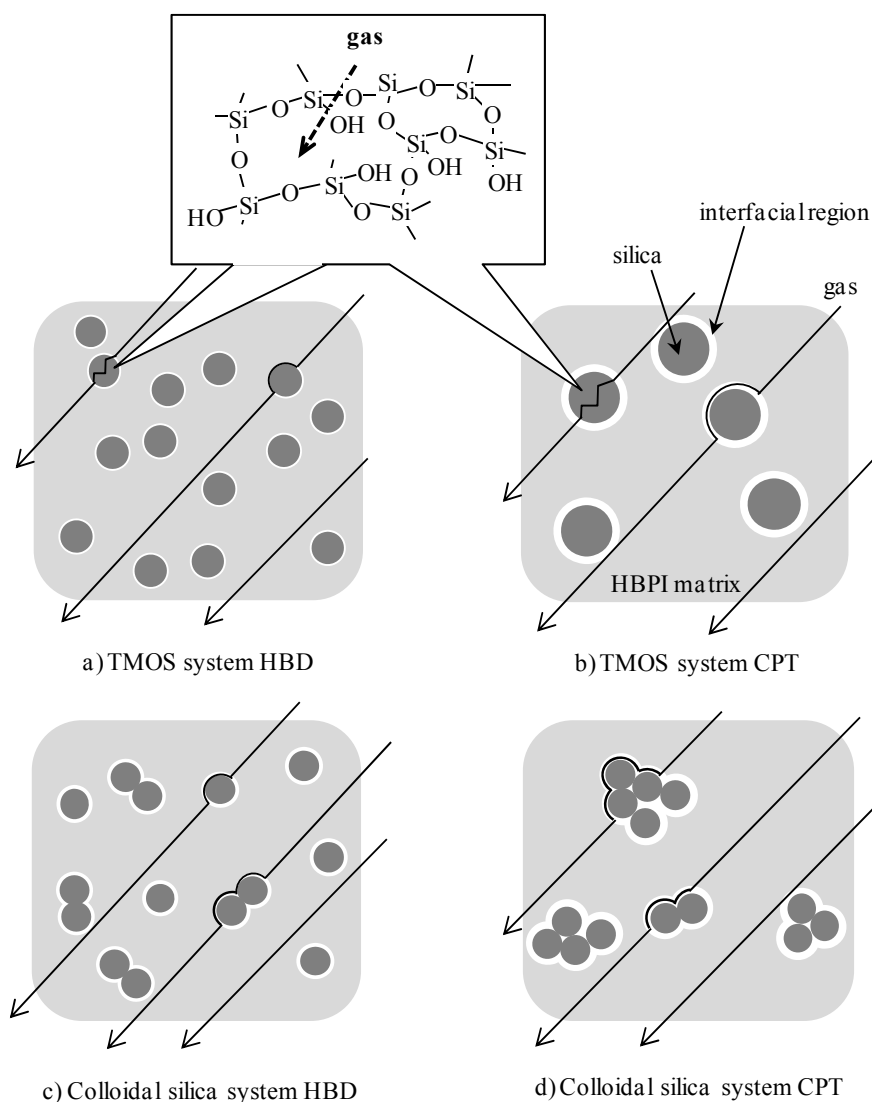
4. Conclusions

HBPI–silica HBD and CPT membranes were prepared by the sol-gel reaction or the addition of colloidal silica and their general and gas transport properties were investigated.

The ATR FT-IR spectra revealed satisfactory imidization and sufficient formation of three-dimensional Si–O–Si networks in all prepared membranes. They also revealed the existence of the silanol groups in the TMOS system hybrids and composites. The HBPI–silica HBD films maintain high transparency similar to the corresponding pristine HBPIs at high silica content, indicating the favorable dispersion of silica. The T_d^5 values of all prepared HBPI–silica HBDs and CPTs increased with increasing the silica content due to the formation of crosslinks between HBPI and the silica domain, the strong

influence of the introduction of inorganic characteristics, and the radical trap effect of silica. From the DMA and TMA measurements, it was found that the most effective influence of the induction of silica on the thermomechanical property is obtained in the TMOS system HBPI–silica HBD because the interaction of the HBPI and the silica domain is stronger than for other hybrids and composites. The gas permeability and CO_2/CH_4 selectivity of the HBPI–silica HBD and CPT membranes prepared via the sol-gel reaction with TMOS increased with increasing silica content. On the other hand, the $\alpha(CO_2/CH_4)$ of the HBPI–silica HBD and CPT with the colloidal silica slightly decreases with increasing CO_2 permeability. From these results, we propose a gas transport mechanism in the HBPI–silica HBD and CPT membranes as follows; The increases in gas permeability and CO_2/CH_4 selectivity of the HBPI–silica HBD and CPT membranes prepared via the sol-gel reaction with TMOS are caused by the contribution of both of the additional formed free volume elements around the polymer–silica interfacial region. This provides a diffusion path and Langmuir-type sorption site for gas molecules, and the formation of amorphous silica via the sol-gel reaction which has a molecular sieving function.

Acknowledgments

Conflicts of Interest

The author declares no conflict of interest.

References

1. Cornelius, C.; Hibshman, C.; Marand, E. Hybrid organic–inorganic membranes. *Sep. Purif. Technol.* **2001**, *25*, 181–193.
2. Kickelbick, G. *Hybrid Materials*; Wiley-VCH: Weinheim, Germany, 2007.
3. Zou, H.; Wu, S.; Shen, J. Polymer/silica nanocomposites: Preparation, characterization, properties, and applications. *Chem. Rev.* **2008**, *108*, 3893–3957.
4. Cornelius, C.J.; Marand, E. Hybrid silica–polyimide composite membranes gas transport properties. *J. Membr. Sci.* **2002**, *202*, 97–118.
5. Ragosta, G.; Musto, P. Polyimide/silica hybrids via the sol-gel route: High performance materials for the new technological challenges. *Express Polym. Lett.* **2009**, *3*, 413–428.
6. Romero, A.I.; Parentis, M.L.; Habert, A.C.; Gonzo, E.E.; Synthesis of polyetherimide/silica hybrid membranes by the sol-gel process: Influence of the reaction conditions on the membrane properties. *J. Mater. Sci.* **2011**, *46*, 4701–4709.
7. Boroglu, M.S.; Gurkaynak, M.A. The preparation of novel silica modified polyimide membranes: Synthesis, characterization, and gas separation properties. *Polym. Adv. Technol.* **2011**, *22*, 545–553.
8. Kim, Y.H. Hyperbranched polymers 10 years after. *J. Polym. Sci. A Polym. Chem.* **2004**, *36*, 1685–1698.

9. Gao, C.; Yan, D. Hyperbranched polymers: From synthesis to applications. *Prog. Polym. Sci.* **2004**, *29*, 183–275.

10. Suzuki, T.; Yamada, Y. Characterization of 6FDA-based hyperbranched and linear polyimide–silica hybrid membranes by gas permeation and [129]Xe NMR measurements. *J. Polym. Sci. B Polym. Phys.* **2006**, *44*, 291–298.

11. Suzuki, T.; Yamada, Y.; Sakai, J. Gas transport properties of ODPA-TAPOB hyperbranched polyimide–silica hybrid membranes. *High Perform. Polym.* **2006**, *18*, 655–664.

12. Suzuki, T.; Yamada, Y. Effect of end group modification on gas transport properties of 6FDA-TAPOB hyperbranched polyimide–silica hybrid membranes. *High Perform. Polym.* **2007**, *19*, 553–564.

13. Suzuki, T.; Yamada, Y. Synthesis and gas transport properties of novel hyperbranched polyimide–silica hybrid membranes. *J. Appl. Polym. Sci.* **2013**, *127*, 316–322.

14. Suzuki, T.; Yamada, Y.; Itahashi, K. 6FDA-TAPOB hyperbranched polyimide–silica hybrids for gas separation membranes. *J. Appl. Polym. Sci.* **2008**, *109*, 813–819.

15. Miki, M.; Suzuki, T.; Yamada, Y. Structure–property relationships of hyperbranched polyimide–silica hybrid membranes with different degrees of modification. *J. Appl. Polym.* **2013**, *130*, 54–62.

16. Takeichi, T.; Stille, J.K. Star and liner imide oligomers containing reactive end caps: Preparation and thermal properties. *Macromolecules* **1986**, *19*, 2093–2102.

17. Prabhakar, R.S.; Freeman, B.D.; Roman, I. Gas and vapor sorption and permeation in poly(2,2,4-trifluoro-5-trifluoromethoxy-1,3-dioxole-*co*-tetrafluoroethylene). *Macromolecules* **2004**, *37*, 7688–7697.

18. Muruganandam, N.; Koros, W.J.; Paul, D.R. Gas sorption and transport in substituted polycarbonates. *J. Polym. Sci. B Polym. Phys.* **1987**, *25*, 1999–2026.

19. Morisato, A.; Shen, H.C.; Sankar, S.S.; Freeman, B.D.; Pinnau, I.; Casillas, C.G. Polymer characterization and gas permeability of poly(1-trimethylsilyl-1-propyne) [PTMST], poly(1-phenyl-1-propyne) [PPP], and PTMSP/PPP blends. *J. Polym. Sci. B Polym. Phys.* **1996**, *34*, 2209–2222.

20. Weinkauf, D.H.; Kim, H.D.; Paul, D.R. Gas transport properties of liquid crystalline poly(*p*-phenyleneterephthalamide). *Macromolecules* **1992**, *25*, 788–796.

21. Chen, H.; Yin, J. Synthesis and characterization of hyperbranched polyimides with good organosolubility and thermal properties based on new triamine and conventional dianhydrides. *J. Polym. Sci. A Polym. Chem.* **2002**, *40*, 3804–3814.

22. Fang, J.; Kita, H.; Okamoto, K. Hyperbranched polyimides for gas separation applications. 1. Synthesis and characterization. *Macromolecules* **2000**, *33*, 4639–4646.

23. Hibshman, C.; Cornelius, C.J.; Marand, E. The gas separation effects on annealing polyimide–organosilicate hybrid membranes. *J. Membr. Sci.* **2003**, *211*, 25–40.

24. Tomokiyo, N.; Yamada, Y.; Suzuki, T.; Oku, J. Preparation and characterization of hyperbranched polyimide–colloidal silica hybrids. *Polym. Prep. Jpn.* **2006**, *55*, 5175–5176.

25. Suzuki, T.; Yamada, Y.; Tsujita, Y. Gas transport properties of 6FDA-TAPOB hyperbranched polyimide membrane. *Polymer* **2004**, *45*, 7167–7171.

26. Suzuki, T.; Yamada, Y. Physical and gas transport properties of novel hyperbranched polyimide–silica hybrid membranes. *Polym. Bull.* **2005**, *53*, 139–146.

27. Yano, K.; Usuki, A.; Okada, A. Synthesis and properties of polyimide–clay hybrid films. *J. Polym. Sci. A Polym. Chem.* **1997**, *35*, 2289–2294.

28. Park, H.B.; Kim, J.K.; Nam, S.Y.; Lee, Y.M. Imide-siloxane block copolymer/silica hybrid membranes: Preparation, characterization and gas separation properties. *J. Membr. Sci.* **2003**, *220*, 59–73.

29. Merkel, T.C.; Freeman, B.D.; Spontak, R.J.; He, Z.; Pinnau, I.; Meakin, P.; Hill, A.J. Ultrapermeable, reverse-selective nanocomposite membranes. *Science* **2002**, *296*, 519–522.

30. Merkel, T.C.; Toy, L.G.; Andrady, A.L.; Gracz, H.; Stejskal, E.O. Investigation of enhanced free volume in nanosilica-filled poly(1-trimethylsilyl-1-propyne) by ^{129}Xe NMR spectroscopy. *Macromolecules* **2003**, *36*, 353–358.

31. Andrady, A.L.; Merkel, T.C.; Toy, L.G. Effect of particle size on gas permeability of filled superglassy polymers. *Macromolecules* **2004**, *37*, 4329–4331.

32. Hill, R.J. Diffusive permeability and selectivity of nanocomposite membranes. *Ind. Eng. Chem. Res.* **2006**, *45*, 6890–6898.

33. Hill, R.J. Reverse-selective diffusion in nanocomposite membranes. *Phys. Rev. Lett*. **2006**, *96*, 216001:1–26001:4.

34. Zhang, Q.G.; Liu, Q.L.; Zhu, A.M.; Xiong, Y.; Zhang, X.H. Characterization and permeation performance of novel organic-inorganic hybrid membranes of poly(vinyl alcohol)/ 1,2-bis(triethoxysilyl)ethane. *J. Phys. Chem. B* **2008**, *112*, 16559–16565.

35. Okamoto, K.; Tanaka, K.; Kita, H.; Ishida, M.; Kakimoto, M.; Imai, Y. Gas permeability and permselectivity of polyimides prepared from 4,4′-diaminotriphenylamine. *Polym. J*. **1992**, *24*, 451–457.

36. Freeman, B.D. Basis of permeability/selectivity tradeoff relations in polymeric gas separation membranes. *Macromolecules* **1992**, *32*, 375–380.

37. Robeson, L.M. Correlation of separation factor *versus* permeability for polymeric membranes. *J. Membr. Sci.* **1991**, *62*, 165–185.

38. Robeson, L.M. The upper bound revisited. *J. Membr. Sci.* **2008**, *320*, 390–400.

39. Fang, J.; Kita, H.; Okamoto, K. Gas permeation properties of hyperbranched polyimide membranes. *J. Membr. Sci.* **2001**, *182*, 245–256.

40. Kim, T.H.; Koros, W.J.; Husk, G.R.; O'brien, K.C. Relationship between gas separation properties and chemical structure in a series of aromatic polyimides. *J. Membr. Sci.* **1998**, *37*, 45–62.

41. Boehme, R.F.; Cargill, G.S. III. X-ray Scattering Measurements Demonstrating In-Plane Anisotropy in Kapton Polyimide Films; In *Polyimides*; Mittal, K.L., Ed.; Plenum Press: New York, NY, USA, 1984.